Dual-scale study of pre-damage, water boundary conditions and frost interaction in concrete

N.B. When citing this work, cite the original published paper.

(article starts on next page)

Dual-scale study of pre-damage, water boundary conditions and frost interaction in concrete

Lang-Zi Chang · **Katja Frid** · **Roland Kruse** ·
Ralf Jänicke · **Karin Lundgren**

Abstract This study investigated the interactive effects of pre-damage, water boundary conditions, and internal frost damage on concrete at dual-scale. The pre-damage included pre-cracking, which has not been studied experimentally before, and pre-compressive damage. Concrete specimens underwent pre-damage and had varied water boundary conditions during Freeze-Thaw Cycles (FTC). At the macro-scale, wedge-splitting tests combined with Digital Image Correlation (DIC) were conducted to assess post-FTC strength and fracture behaviour. At the meso-scale, X-ray CT scanning was employed to identify internal crack patterns. Results reveal that at the macro-scale, significant interaction between pre-damage and frost damage reduced splitting tensile strength compared to the internal frost damage alone. Besides, increased water exposure during FTCs reduced both splitting tensile strength and compressive strength, with a less pronounced reduction in splitting tensile strength. It also led to a diffuse crack pattern and increased tensile ductility. At the meso-scale, specimens subjected to the interactive effects of pre-damage and internal frost damage exhibited cracks along aggregate-cement interfaces and within the cement paste. Reference specimens displayed no internal cracks, while specimens exposed to only FTCs showed only cracks along aggregate-cement interfaces. Full submersion of specimens during FTCs induced more internal cracks than solely water on top. These findings on the interactions between pre-damage, water boundary conditions, and internal frost damage offer insight into the causes of frost damage, vital for the design and assessment of concrete structures in frost-prone environments. Furthermore, the results of these dual-scale tests can be used as a test case for the development of upscaling numerical models describing heat transfer and frost degradation in concrete.

L.-Z. Chang (✉) · K. Lundgren
Department of Architecture and Civil Engineering,
Chalmers University of Technology, 41258 Gothenburg,
Sweden
e-mail: langzi.chang@chalmers.se

K. Frid
Department of Materials Science and Applied
Mathematics, Malmö University, 21119 Malmö, Sweden

R. Kruse · R. Jänicke
Institute of Applied Mechanics, Technische Universität
Braunschweig, 38106 Braunschweig, Germany

1 Introduction

Recent climate change has increased the frequency of Freeze-Thaw Cycles (FTCs) in cold regions, escalating the risk for existing concrete structures [1, 2]. One of the major types of damage caused by FTCs

in concrete is internal frost damage [3]. In the freezing phase of one FTC, ice confined within the pore system of concrete undergoes expansion, inducing tensile stresses and thereby forming micro-cracks that interconnect pores. Subsequent thawing prompts the ingress of water into these newly formed micro-cracks and pores, with the water freezing and expanding in the next freezing phase. This cyclic process gradually undermines the durability and even structural safety of concrete [4, 5]. In real-world scenarios, the durability of concrete structures is influenced by the interplay of a range of factors. The combined impact of FTCs, pre-existing damage (pre-damage) and the presence of water in the surrounding environment can lead to severe deterioration of concrete structures beyond the effect of individual sources of damage [6–8].

In practical engineering, the combined effects of pre-damage and internal frost damage on concrete are commonly observed [9]. For example, concrete beams and slabs often crack as a result of bending and drying. This process may lead to pre-existing surface cracking, also known as pre-cracking. Such cracking is typically characterised by a few large cracks. These cracks may occur concurrently with internal frost damage or develop beforehand. For concrete components under significant compression, prior compressive stresses can induce internal micro-damage (pre-compressive damage), characterised by numerous small cracks, which may interact with future FTCs. Lu et al. [10] found that subjecting concrete to fatigue compression loading before FTCs resulted in greater internal damage compared to the reverse sequence, indicating that pre-damage potentially exacerbates internal frost damage in concrete. Numerous studies have investigated the isolated effects of FTCs on concrete, revealing reductions in tensile strength, compressive strength, initial stiffness, and alterations in fracture behaviour [4, 11–14], research on the combined impact of pre-damage and internal frost damage has been relatively limited. Sun et al. [15, 16] conducted experiments involving simultaneous bending load and FTCs on fibre-reinforced small concrete beams, observing accelerated damage progression and increased internal frost damage. Additionally, Bao et al. [17] applied compressive loads to concrete cubes before subjecting them to FTCs, noting exacerbated concrete deterioration compared to specimens without pre-compressive damage. Although previous studies highlight the potential negative effects of pre-damage on internal frost damage, there is a lack of studies examining these interactive effects in concrete, both on the surface and internally. Moreover, the combined impact of pre-existing cracks induced by splitting forces and internal frost damage, common in cold regions, has not been experimentally studied. This gap hinders a comprehensive understanding of concrete durability under the complex combination of external loading and FTCs in real-world scenarios.

Water boundary conditions significantly influence internal frost damage in concrete by affecting the degree of saturation through variations in surrounding water levels. According to theories proposed by Fagerlund [18], internal frost damage occurs only when the saturation of concrete exceeds a critical threshold. Further, experimental tests with different water boundary conditions have yielded conflicting findings, complicating the understanding of their interaction with FTCs. For instance, a laboratory study by Hassanzadeh and Fagerlund [19] found no internal frost damage in large concrete beams ($4.4 \times 0.5 \times 0.2$ m^3) after being submerged in water tanks for two years and exposed to two FTCs, while Rong et al. observed a significant reduction in load-bearing capacity when water was sprayed on beam ($1.2 \times 0.25 \times 0.15$ m^3) surfaces during FTCs [20]. Other experiments involved smaller specimens (sectional size of 100 mm) entirely submerged in water [4, 21–24], with few studies directly comparing different water boundary conditions and their interactions with FTCs. Thus, there remains a notable gap in knowledge regarding the influence of water boundary conditions.

To better understand internal frost damage in concrete, dual-scale experimental studies are essential. Here, "dual-scale" refers to investigations encompassing both macro-scale and meso-scale. At the macro-scale (structural or component level, above 10 mm), concrete is considered a homogenised material, whereas at the meso-scale (material level, 1–5 mm), it is necessary to distinguish the individual constituents of concrete, such as aggregates and the cementitious matrix [25]. At the macro-scale, mechanical tests, such as wedge-splitting and compression tests, assess the impact of frost damage on tensile strength/fracture behaviour and compressive strength, respectively [4, 11, 12, 26–31]. Digital Image Correlation (DIC) can

supplement these tests, providing an estimate of the displacement fields and making crack propagation on concrete surfaces visible [4, 24]. Regarding the meso-scale, observing internal crack propagation is crucial in understanding the nature of frost damage inside the concrete. With this aim, X-ray Computed Tomography Scanning (X-ray CT scanning) is a non-destructive technique capable of distinguishing aggregates from cement paste [32–34] and highlighting internal cracks [29, 35–38]. However, studies combining DIC for macro-scale fracture behaviour and X-ray CT imaging for meso-scale crack propagation are lacking. This is particularly true for research on the interaction between pre-damage, water boundary conditions, and internal frost damage in concrete.

This experimental study aims to investigate the interaction between pre-damage, water boundary conditions and internal frost damage at dual-scale. Concrete specimens were pre-damaged under tension or compression and thereafter subjected to various water boundary conditions during FTCs. Electronic probes embedded in the concrete monitored temperature changes throughout the FTC procedure. After FTCs, wedge-splitting and compression tests were performed, accompanied by DIC, to investigate the interactive effects of pre-damage, water boundary conditions and internal frost damage on tensile strength, fracture behaviour and compressive strength of concrete at the macro-scale. Subsequently, X-ray CT scanning was applied on drilled cores to observe the cracking propagation inside the concrete at the meso-scale. The findings of this study contribute to the field of structural and construction engineering by offering insights that can inform the design of more resilient concrete structures in cold regions and the development of maintenance strategies for concrete components.

2 Experimental program

The experimental program consisted of four parts: preparation, Freeze-Thaw Cycles (FTC), mechanical testing (macro-scale) and X-ray CT imaging (meso-scale). During the preparation stage of the specimens (from casting till the start of FTCs), pre-damage in the form of pre-cracking or pre-compressive damage was applied to some of the specimens. Pre-cracking mimics existing surface cracks in structures, corresponding to scenarios such as beams or slabs cracked due to bending and drying. Pre-compression aims at inducing internal micro-damage, corresponding to scenarios where structural components are subjected to significant compressive stresses. During the FTC stage, various water boundary conditions were applied to the specimens. For some specimens, water was maintained on their top surfaces, to mimic structures such as top surfaces of roads and bridges in direct contact with surrounding water. Other specimens were fully submerged in water, to mimic hydraulic structures such as docks and dams. After the FTC stage, mechanical tests, namely, wedge-splitting and compression tests, were performed to assess the tensile strength/fracture behaviour and compressive strength of the concrete, respectively. Finally, cores were drilled out of the specimens and subjected to X-ray CT scanning to examine cracks inside the concrete.

A schematic diagram of the experimental process is presented in Fig. 1.

2.1 Preparation of the specimens

Concrete with a water-cement ratio of 0.5 was cast in one batch, see Table 1 for the mix composition. This mix was intended to mimic concrete in old existing concrete structures. Therefore, no air-entrainer or superplasticizer was added. In the laboratory, concrete was prepared following a standardised

Fig. 1 Timeline of the experiments (in days)
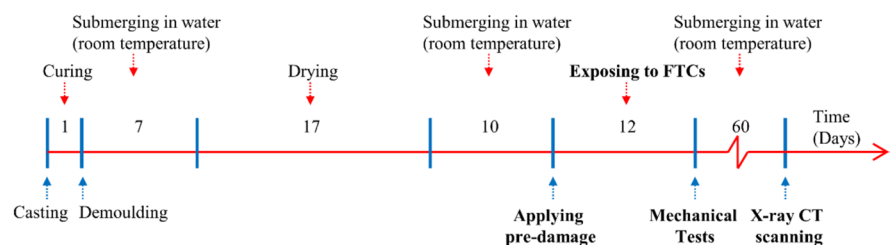
Table 1 Concrete mix composition

Constituents	Mix (kg/m^3)
Cement (CEM I 42.5 N)	480
Tap water	240
Fine aggregate (0–4 mm)	600
Coarse aggregate (4–10 mm)	900

mixing procedure. Cement, fine aggregates, and coarse aggregates were first dry-mixed in a concrete mixer for 2 min to ensure uniform distribution. Subsequently, water was gradually added, and the mixture was wet-mixed for 3 min to achieve homogeneity. The fresh concrete was then transferred to moulds immediately after mixing to prevent segregation or loss of workability. During casting, the concrete was

poured into the mould in two layers, with each layer compacted using an electronic concrete vibrator for 20 s. 24 h after casting, all specimens were removed from the mould and submerged in tap water at 20 °C for 7 days. Then they were dried in two identical climate chambers at 20 °C and a relative humidity of 30% for 17 days followed by 10 days of submerging in tap water at 20 °C. Similar sequence can be found in [4]. After these preparations, the specimens were pre-damaged and put in climate chambers to undergo FTCs.

The geometries of the specimens are presented in Fig. 2a and b. For some specimens, grooves and notches were cast and cut for wedge-splitting tests. The geometry follows the one introduced in [39, 40]. For the other specimens, 100 mm^3 concrete cubes were cast. Before the FTC procedure, pre-cracking or

Fig. 2 Geometry of specimens for wedge-splitting tests (**a**) and cubic specimens (**b**) (unit in mm). Criteria for applying pre-cracking (**c**) and pre-compressive damage (**d**)

(a)   (b)

(c)   (d)
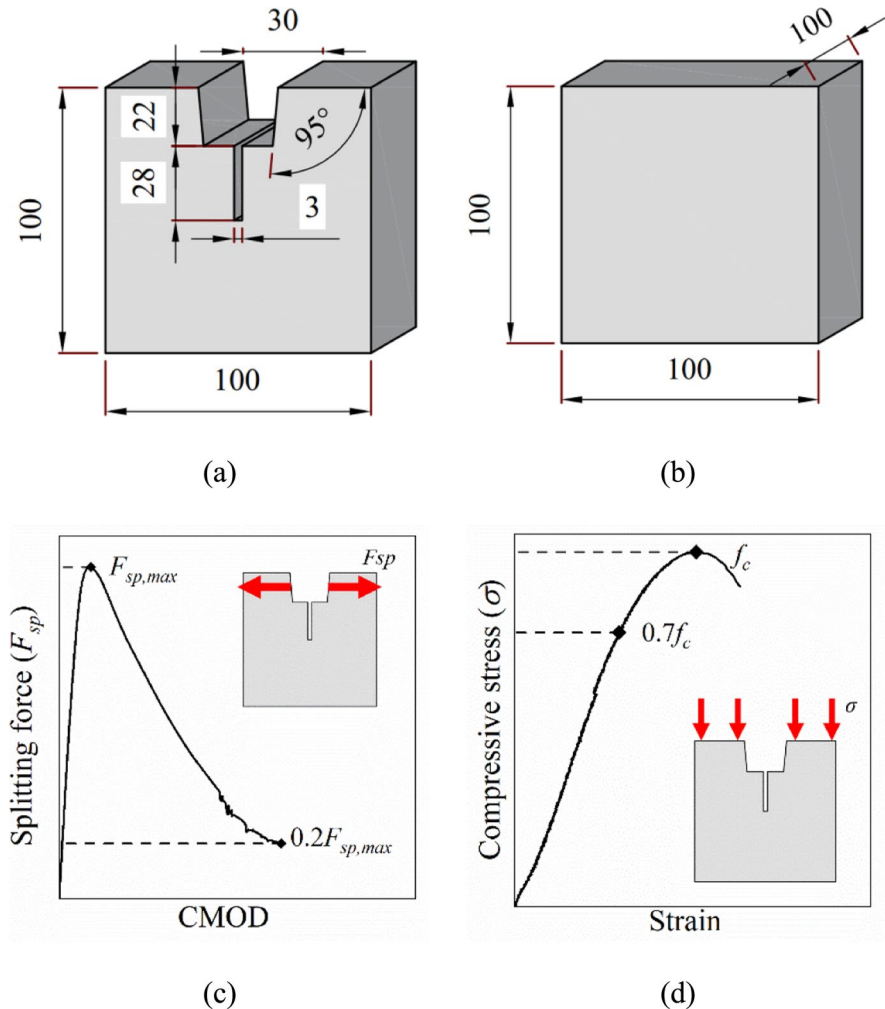
pre-compressive damage was applied to some specimens intended for the wedge-splitting tests. To generate a pre-crack, specimens were split to an extent when the splitting force surpassed its peak ($F_{sp,\ max}$) and dropped to 20% of the peak load (Fig. 2c). This threshold was selected to avoid the sharp drop of the splitting force right after the peak load and to result in a constant crack width among different specimens. To apply pre-compressive damage, a stress of 70% of the compressive strength (f_c), as determined using specimens not subjected to FTC, was applied to the specimens on their top surfaces (Fig. 2d). This value reaches the limit set by Eurocode 2, where the compressive strength of concrete needs to be divided by a factor of 1.5 considering persistent loading for ultimate limit states [41]. Besides, with such a stress/compressive strength ratio, internal cracks may form, known to influence internal frost damage in concrete [17].

The testing scheme and notation of the specimens are shown in Table 2. The notation of the specimens consisted of four characters. The first character denotes the geometries of specimens: cubic (C) or with grooves and notches for wedge-splitting tests (W). The second character denotes types of pre-damage, namely, no pre-damage (N), pre-cracking (P) or pre-compressive damage (C). The third character indicates the number of surfaces exposed to water, in this study, no water (0), with water maintained on top (1) or fully submerged in water (6). The last character refers to the serial number of a specimen in one group. In this scheme, W–N-0-X and C-N-0-X were reference specimens without pre-damage or exposure to FTCs. For cubic specimens, three samples in each group underwent compression testing without X-ray CT scanning. The fourth sample in each group was excluded from compression testing and designed only to X-ray CT scanning. This approach ensured that samples unaffected by compressive damage were available for X-ray CT scanning, to detect damage resulting solely from FTCs.

2.2 Freezing–thawing cycles

During the FTC stage, specimens were placed in two identical climate chambers and exposed to repeated FTCs. Additional reference specimens were fully submerged in water at 20 °C (no frost damage). Each FTC lasted 24 h and followed the air temperature regime recommended by RILEM TC 176-IDC [42] (see Fig. 3). The entire test consisted of 12 FTCs.

The water boundary conditions of the specimens are presented in Fig. 4. For specimens with water maintained on top, rubber tape surrounded the top edges. Silicone was filled between the rubber tapes and concrete to prevent water leakage. As can be seen, the wedge and notch of these specimens were filled with water during freezing. The whole specimen was covered with a thin layer of plastic foil to prevent the water from evaporating (Fig. 4a). For specimens fully submerged in water, each specimen was placed in an individual plastic container with a size of $110 \times 110 \times 110$ mm^3 (Fig. 4b). In both cases, tap water was used. The water layer over the concrete surfaces was controlled to be 5 mm. In this way, the water boundary conditions were well-defined, and are thus ideal for calibrating numerical models of heat

Table 2 Testing scheme: overview of samples and test conditions in the FTC tests

Geometry of specimens	Notation	Quantity	Pre-damage	Water boundary condition during FTCs	Tests after FTCs
Cubic	C-N-0-X	4	None	In water, room temperature	Compression tests / X-ray CT scanning
	C-N-6-X	4	None	fully submerged in water	
	C-N-1-X	4	None	water maintained on top	
With grooves and notches for wedge-splitting tests	W-N-0-X	4	None	In water, room temperature	Wedge-splitting tests
	W-N-6-X	4	None	fully submerged in water	
	W-P-6-X	4	Pre-cracked	fully submerged in water	
	W-C-6-X	4	Compressed	fully submerged in water	
	W-N-1-X	4	None	water maintained on top	
	W-P-1-X	4	Pre-cracked	water maintained on top	

Additional samples were used to determine the properties of the undamaged material
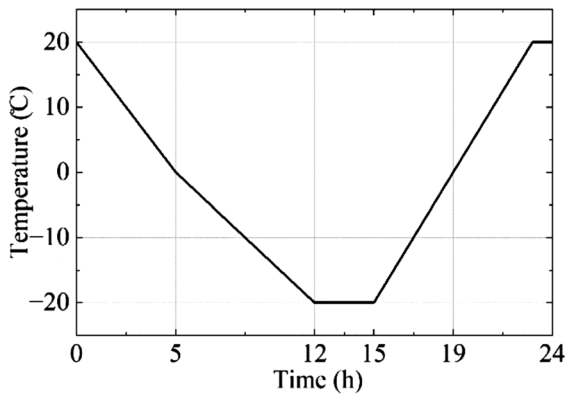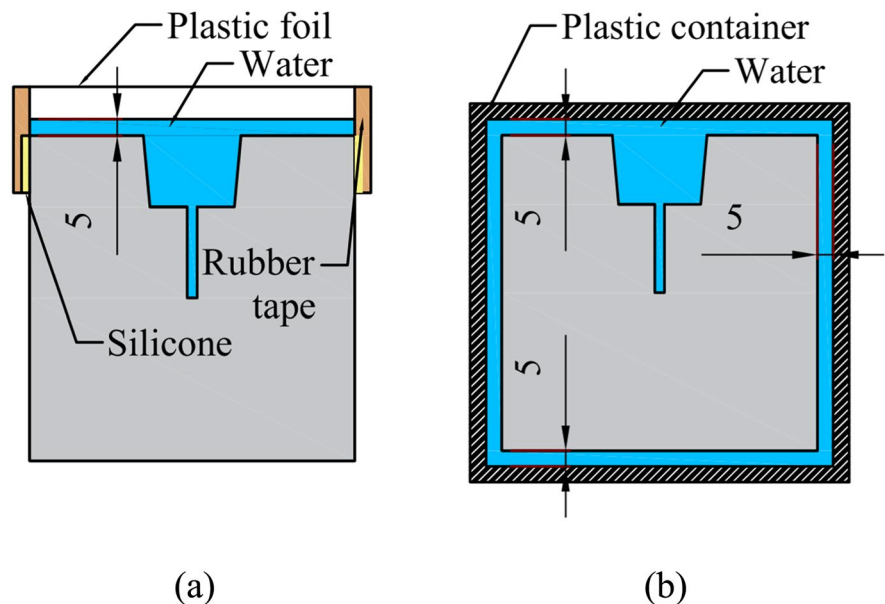
Fig. 3 One FTC, as recommended by RILEM Standard [42]

transfer and mechanical degradation in concrete subjected to internal frost damage.

To monitor the temperature change within the concrete, temperature probes (Fig. 5a) were cast in two specimens, C-N-1–4 and C-N-6–4 (Fig. 5b). For C-N-1–4, a specimen with water maintained on its top surface, three probes were placed at 25 mm, 50 mm, and 75 mm beneath the centre of its top surface (Fig. 5c). For C-N-6–4, a specimen fully submerged in water, two probes were placed at 25 mm and 50 mm beneath the centre of its top surface (Fig. 5d). For both specimens, an additional probe was placed at the centre of one of its side surfaces.

A temperature logger (HIOKI LR8431-20) was connected to the temperature probes to record the temperature change in concrete. The precision was 1 °C.

2.3 Mechanical tests

The wedge-splitting tests were carried out on specimens with grooves and notches [39], see Fig. 2a. Two steel roller bearings were placed on either side of the groove at the top of the specimen. A wedge with an angle of 30° was inserted into the roller bearings. During the tests, the vertical load, F_v, applied on the top of the wedge, caused horizontal splitting force, F_{sp}. A clip gauge was placed in the groove to monitor the Crack Mouth Opening Displacement (CMOD). The wedge-splitting tests were conducted in vertical displacement control at a rate of 0.25 mm/min. Readers are referred to [39] for details about the testing configurations of the wedge-splitting test. To facilitate monitoring the crack pattern during the wedge-splitting tests, Digital Image Correlation (DIC) was applied. The DIC photos were captured at a rate of 100 photos per minute, and the subsequent results were processed by GOM Correlate 2018. For the compression test, the loading rate was 0.6 MPa/s, following the procedure recommended in Eurocode EN 12390-3:2019 [43].

Fig. 4 Water boundary conditions of **a** specimens with water maintained on top; and **b** specimens fully submerged in water (unit in mm)

(a)   (b)

Fig. 5 a Temperature probe; **b** temperature probes cast in concrete; **c** positions of temperature probes in C-N-1-4; **d** positions of temperature probes in C-N-6-4. (Unit in mm.)

(a)

(b)


(c)

(d)
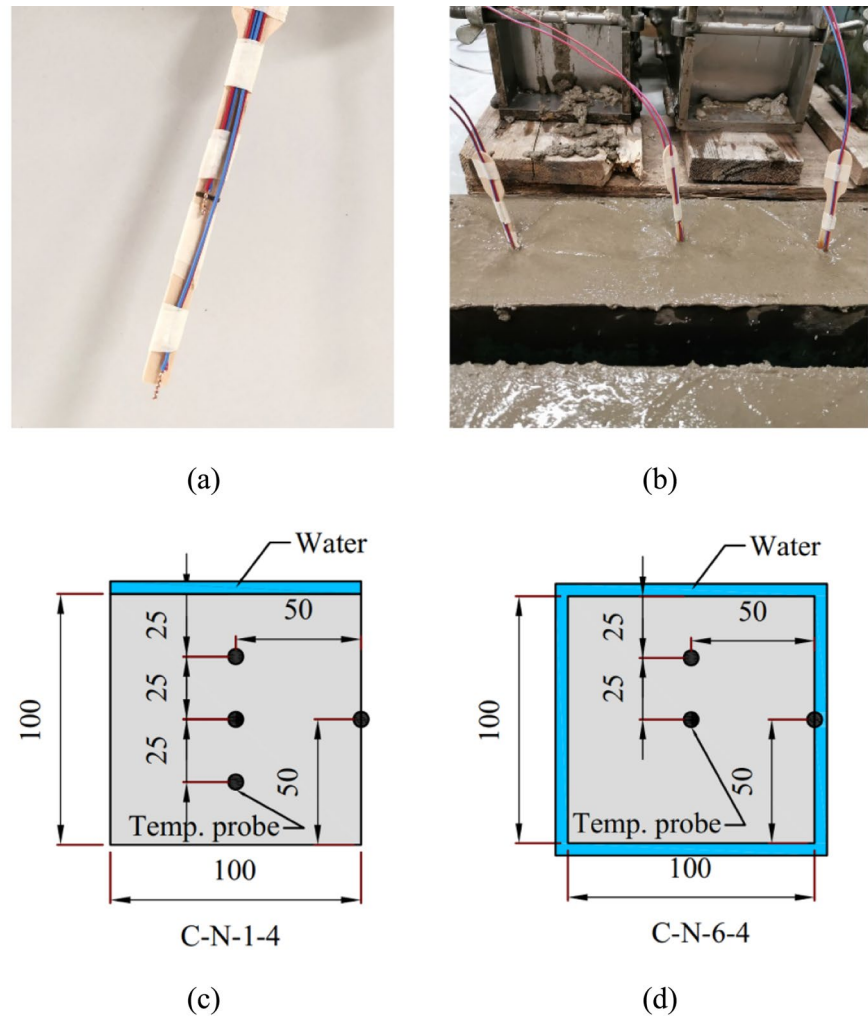
2.4 X-ray CT scanning

Following mechanical testing, cylindrical cores were water-drilled out of the specimens for X-ray CT scanning to assess potential internal cracks resulting from frost damage. The concrete cores had a diameter of 12 mm, with drilling performed at the location depicted in Fig. 6a. Cubic specimens C-N-0-4, C-N-6-4, and C-N-1-4 were excluded from compression tests but were prepared for X-ray CT scanning after exposure to FTCs. X-ray CT scanning was conducted at 150 kV and 66 µA beam current, with 1.2 mm aluminium pre-filter, at 4 fps with 4 averages and a voxel size of 9.7 µm. Subsequent analysis of the 3D image reconstructed by manufacturer-supplied software used open-source software ImageJ [44]. Initially, adjustments were made to the brightness and contrast of the scanned images, followed by unsharp masking to enhance contrast between cracks and concrete. Finally, a uniform threshold using the IsoData method [45] was applied to highlight the cracks. The entire image processing procedure is illustrated in Fig. 6b-d.

3 Experimental results and discussion

In this section, experimental results are presented and discussed concerning the interaction between pre-damage, water boundary conditions, and internal frost damage. First, temperature changes within the concrete are discussed. Then, the discussion focuses on macro-scale observations derived from mechanical tests and DIC analysis, as well as observations on the

Drill cores; Modify brightness/contrast; Set threshold
X-ray CT scan Unsharp mask

(a)   (b)   (c)   (d)
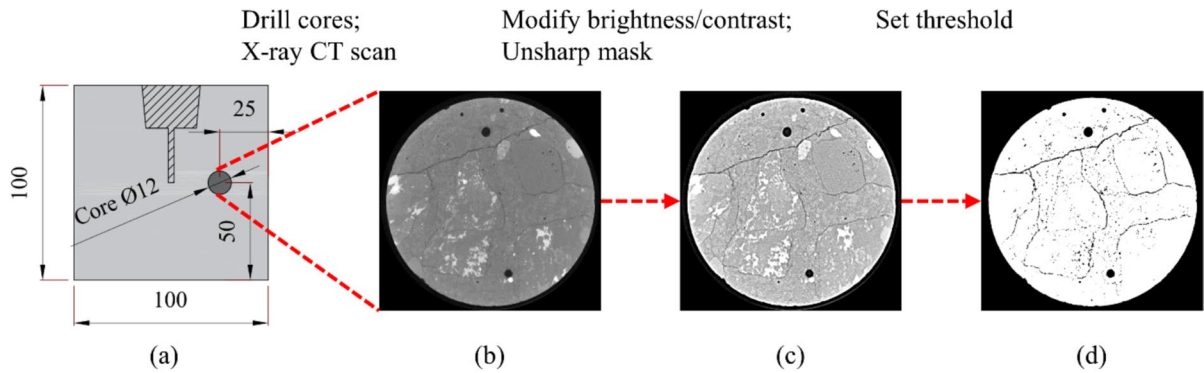
Fig. 6 **a** Drilling position of concrete cores of specimens for wedge-splitting tests and cubic specimens; **b** original X-ray CT scanning image of a core section; **c** image after adjusting brightness/contrast and unsharp masking; **d** crack pattern highlighted with the set threshold

meso-scale: internal cracks made visible by X-ray CT imaging.

3.1 Temperature change in concrete

Figure 7 illustrates the temperature change in concrete, with the placement of temperature probes detailed in Fig. 5. Note as shown Fig. 5d, two probes were embedded in C-N-6. However, probe C-N-6-4-50 lost its signal during FTCs. Therefore, no data from probe C-N-6–4 is presented in this section. Due to the uniformity of temperature changes across all FTCs, Fig. 7 showcases the temperature change in two representative FTCs. The solid grey curve in Fig. 12 depicts the air temperature within the climate chamber, affirming the successful implementation of programmed FTCs (refer to Fig. 3). During FTCs for the specimen with water maintained on top

(C-N-1–4), the temperature followed a distinct pattern: as environmental temperatures rose, surface temperature (probe C-N-1–4-SURF) increased first, followed by increasing internal temperature from the bottom (probe C-N-1–4-75, away from water) to top (probe C-N-1-4-25, close to top water) of the concrete. During the freezing phase, surface temperature decreased initially, followed by internal temperature reduction from the bottom to the top of the concrete.

For the specimen fully submerged in water (C-N-6), as the environmental temperature rose during each FTC, the surface temperature (probe C-N-6-4-SURF) stabilised at 0 °C before sharply rising to its peak. In contrast, the increase of temperature within the concrete (probe C-N-6-4-25) was more gradual. This is because the melting of the ice consumed the energy from the surrounding environment, leading to no temperature increase. When the melting finished, the

Fig. 7 Temperature change in the climate chamber, on the surface of and inside the specimens C-N-6-4 (blue curves) and C-N-1-4 (red curves). The last digit in the specimen notation corresponds to the location of temperature probes: "SURF" denotes the surface, while numerical values indicate the distance from the top surface
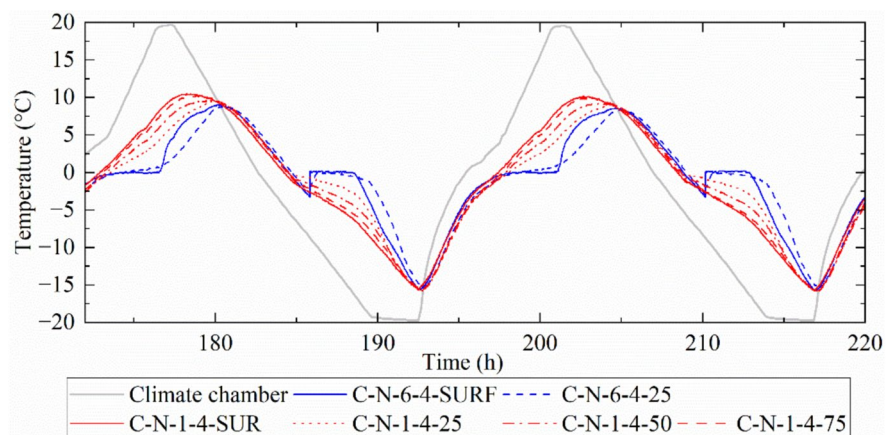
energy was used to increase the temperature. Upon the surface, the ice had the same conditions to melt. Inside the concrete, ice accommodated in pores and cracks of different sizes melted at different temperatures. Therefore, the melting processes on the surface and inside the concrete were different. Upon reaching $-3.3\ °C$ both on the surface and within the concrete during the freezing period of each FTC, temperatures sharply rose back to $0\ °C$, remained stable for approximately 2 h, and then began to decrease once more. This is due to phase transition being exothermic. The produced heat from ice formation increased the temperature since the surrounding air environment could not extract the energy fast enough. Therefore, the temperature stayed at $0\ °C$ (otherwise the ice would melt again) until the energy was released and the temperature restarted to decrease in the concrete. This phenomenon is attributed to the interaction of water with complex solutes dissolved from concrete, pore sizes of concrete and the stochastic process of freezing, altering the crystallisation and freezing process of water. Additionally, similar observations were reported in a study by Pålbrink and Rydman [46] regarding temperature measurements of concrete submerged in water subjected to freeze–thaw cycles.

The presence of internal frost damage in concrete depends on the formation of ice within the concrete. Analysis of temperature change confirms the presence of ice within the concrete. Moreover, extended exposure to $0\ °C$ temperatures during freezing leads to increased ice formation. Consequently, it is inferred that fully submerged samples exhibit greater ice formation compared to those with water only on the top surfaces. This observation aligns with mechanical test findings indicating intensified frost damage in fully submerged samples.

3.2 Macro-scale: splitting tensile strength and fracture behaviour

This section focuses on the combined effects at the macro-scale. Figure 8 presents the Crack Mouth Opening Displacement (CMOD) versus splitting force curves alongside the crack path observed in representative specimens from each testing group, as monitored by DIC during the wedge-splitting tests. In each subplot of the CMOD-splitting force relations, the curves for individual specimens are depicted in grey, while the averaged curves are shown in black.

For pre-cracked specimens within groups W-P-6 and W-P-1, the graphics before and after frost damage are combined into a single plot, with a plus sign denoting the graph from pre-cracking. Results show that the CMOD-splitting force curves exhibit small variations among individual specimens within each group. Crack patterns are shown at the onset of cracking, at peak splitting force, and at the end of wedge-splitting tests. Additionally, crack patterns during wedge-splitting tests following FTCs were recorded for pre-cracked specimens W-P-6 and W-P-1. For these specimens, since no pronounced peak splitting forces were observed in the wedge-splitting tests after FTCs (Fig. 8c and f), crack patterns at an intermediate time point are presented. Frost-damaged specimens exhibited a distinct feature compared to the reference specimen (W-N-0), with crack patterns diffusing in multiple directions, whereas the crack of the reference specimen predominantly propagated unilaterally from the notch tip to the specimen base. Pre-cracked specimens (W-P-6 and W-P-1) initially followed pre-crack paths before diffusing in multiple directions, while cracks in other frost-damaged specimens originated from the notch tip and diffused immediately. This observation supports the hypothesis that pre-cracking leads to a higher saturation rate in surrounding concrete, resulting in more severe internal frost damage and more diffused cracking.

Based on the CMOD-splitting force curves from Fig. 8, average splitting tensile strength (F_{sp}) and their variations within each group are summarised in Table 3. Following frost damage, specimens subjected to pre-cracking (W-P-6 and W-P-1), or pre-compressive damage (W-C-6) display large variations in splitting tensile strength (coefficient of variation (C.o.V.) of 40%, 16.5%, and 36.1%, respectively). This variability can be attributed to non-uniform damage induced by pre-cracking or pre-compressive damage, stemming from the inherent heterogeneity of concrete. Pre-cracking, despite being controlled to exceed the peak force and decrease to 20% of the peak, resulted in divergent cracking paths from the notch tip among specimens. Similarly, pre-compressive damage, although controlled at consistent levels, potentially led to varying patterns of internal damage in concrete. During FTCs, ice expansion within different pre-cracked paths or internally damaged microstructures contributed to diverse splitting forces in subsequent wedge-splitting tests. In contrast, other

(a) Group W-N-0: reference

(b) Group W-N-6: no pre-damage, fully submerged

(c) Group W-P-6: pre-cracked, fully submerged

(d) Group W-C-6: pre-compressed, fully submerged

(e) Group W-N-1: no pre-damage, water on top

(f) Group W-P-1: pre-cracked, water on top
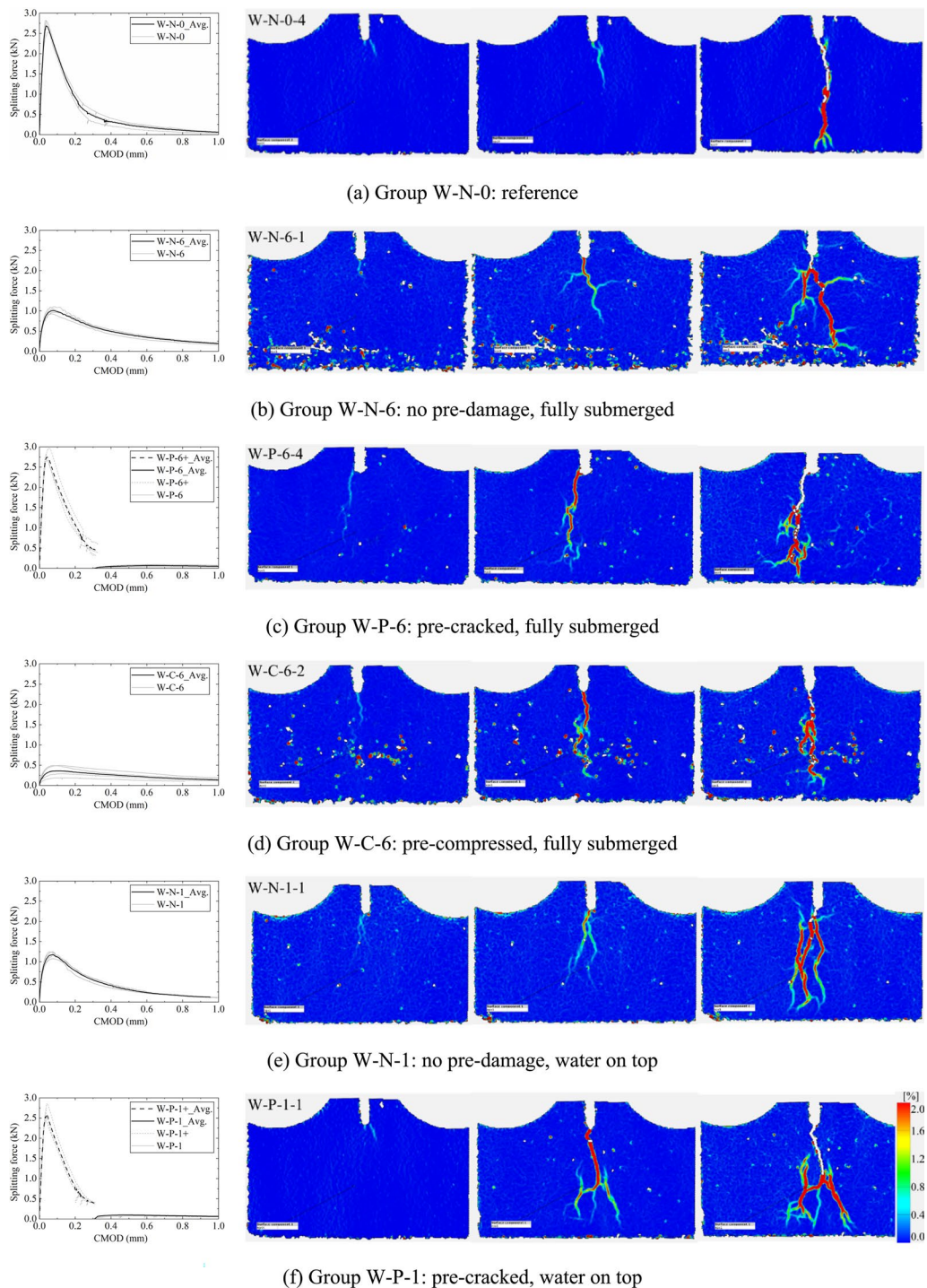
Fig. 8 CMOD-splitting force curves and crack propagation of representative specimens in each group from wedge-splitting tests. Crack patterns at the onset of cracking, at peak force and the end of the test, are shown from left to right in each row. For pre-cracked specimens, W-P-6-4 and W-P-1-1, crack pattern after frost damage rather than at the pre-cracking stage are presented

Table 3 Average splitting tensile strength (F_{sp}) and variation of each tested group

Group		W-N-0	W-N-6	W-P-6	W-P-6+	W-C-6	W-N-1	W-P-1	W-P-1+
Conditions	Pre-damage	No	No	Pre-cracked	(Residual stage of W–P-6)	Pre-compressed	No	Pre-cracked	(Residual stage of W–P-1)
	Water BCs during FTCs	Fully in water but no FTCs	Fully in water	Fully in water		Fully in water	Water on top	Water on top	
Average F_{sp} (kN)		2.72	1.02	2.78	0.07	0.37	1.18	2.64	0.10
Standard variance (kN)		0.14	0.07	0.12	0.03	0.13	0.07	0.17	0.02
Coefficient of variation		5.1%	7.0%	4.4%	39.6%	36.1%	6.0%	6.5%	16.5%

groups including the ones without pre-damage but only FTCs exhibit minimal variance (C.o.V. ranging from 4.4 to 7.0%), indicating uniform casting and negligible differences among individual specimens.

Figure 9 illustrates the impact of pre-cracking, pre-compressive damage, and water boundary conditions on CMOD-splitting force curves. In Fig. 9a and b, it is observed that pre-cracked concrete (W-P-6 and W-P-1) fails to regain its splitting force levels at the end of pre-cracking following FTCs. This suggests that pre-cracking amplifies internal frost damage by facilitating water intrusion into surrounding areas, leading to higher saturation levels and subsequent expansion-induced cracking, thus reducing macro-level splitting force. Another potential explanation for this phenomenon is that the ice in the existing surface cracks expanded during freezing, keeping the cracks developing, therefore leading to a reduction of split-ting tensile strength.

Figure 9c depicts the effect of pre-compressive damage, revealing a 63% and 86% reduction in split-ting tensile strength for specimens fully submerged in water (W-N-6) and pre-compressed and submerged in water (W-C-6), respectively, compared to the refer-ence group (W-N-0). This underscores that pre-com-pressive damage exacerbates internal frost damage by inducing internal cracks, which in turn accommodates more water content. During FTCs, the freezing and expansion of water within these internal cracks inten-sify frost damage, surpassing the severity observed in non-pre-compressed concrete.

Furthermore, Fig. 9d demonstrates the influence of water boundary conditions, with specimens sub-jected to water maintenance on top (W-N-1) and full submersion (W-N-6) exhibiting reductions of 57% and 63% in splitting tensile strength relative to the

reference group (W-N-0). This signifies that increased exposure of concrete surfaces to surrounding water correlates with more severe internal frost damage. Elevated saturation rates due to greater surface expo-sure led to increased cracking induced by ice expan-sion within the concrete, thereby decreasing splitting tensile strengths. Moreover, increased exposure to surrounding water enhanced the ductility of concrete, as evidenced by the comparison between CMOD-splitting force curves in Fig. 9d and crack patterns of W-N-1 and W-N-6 shown in Fig. 8. A possible expla-nation is that frost damage creates internal cracks in the concrete, as demonstrated in the following sec-tions. These cracks lead to increased stress redistribu-tion and energy absorption during fracture, ultimately resulting in greater ductility.

3.3 Macro-scale: compressive strength

This section focuses on the combined effect of water boundary conditions and FTCs on the compressive strength of concrete at the macro-scale. Figure 10 illustrates the compressive strength of cubic speci-mens, including their respective average values within each group. In each group, compression tests were applied to the first three specimens. The fourth speci-men was excluded from compression tests as they were designated for X-ray CT scanning. In compari-son to the reference specimens (C-N-0), the average compressive strength decreased by 18% and 31% for specimens with water on top (C-N-1) and fully sub-merged in water (C-N-6), respectively. Figure 10 also illustrates the failure patterns of specimens follow-ing compression tests. In comparison to the reference group (C-N-0) where minimal spalling was noted, specimens with water maintained on top (C-N-1)
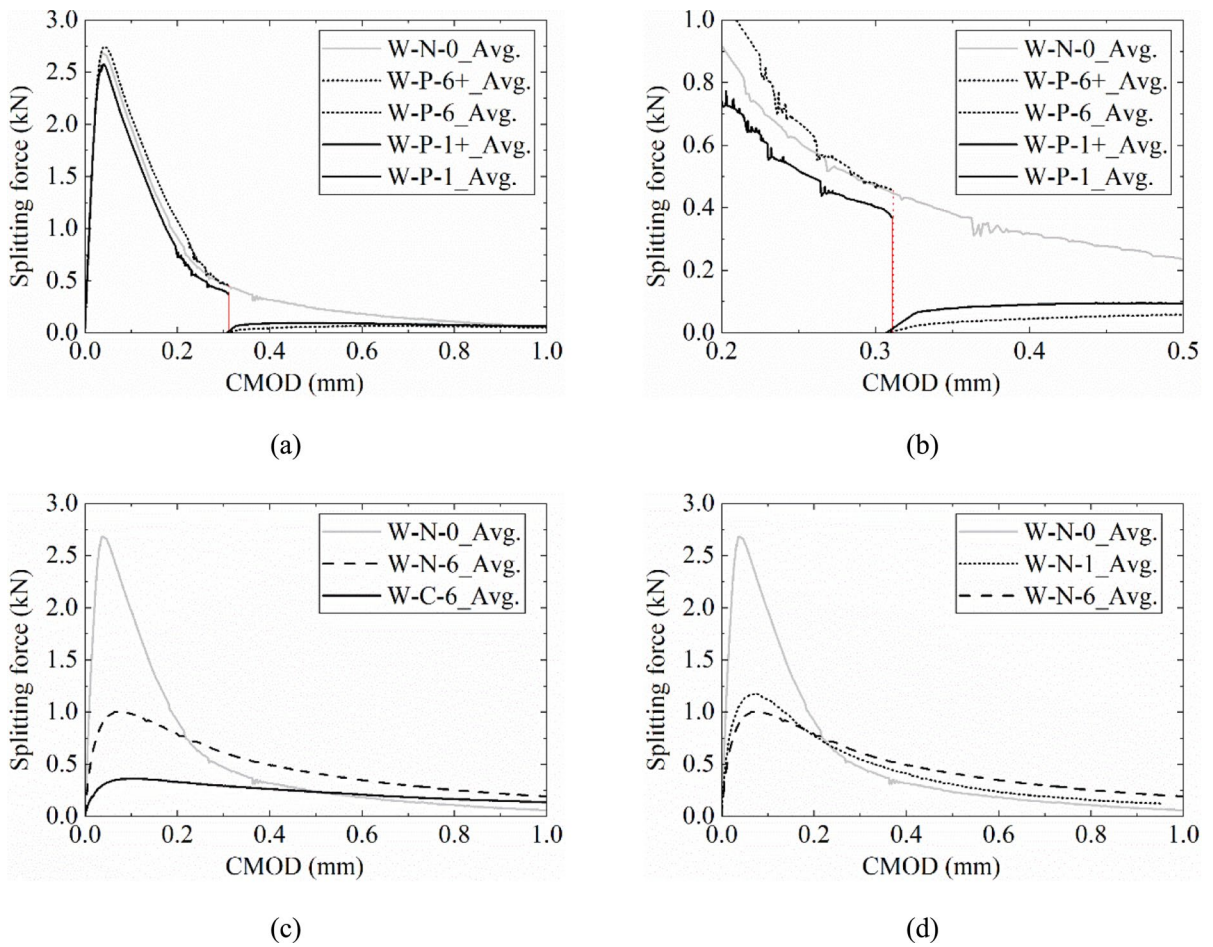
Fig. 9 **a** Comparisons regarding the influence of pre-cracking on frost damage; **b** a zoom-in view. **c** and **d**: comparisons regarding the influence of pre-compressive damage and water boundary conditions on frost damage, respectively
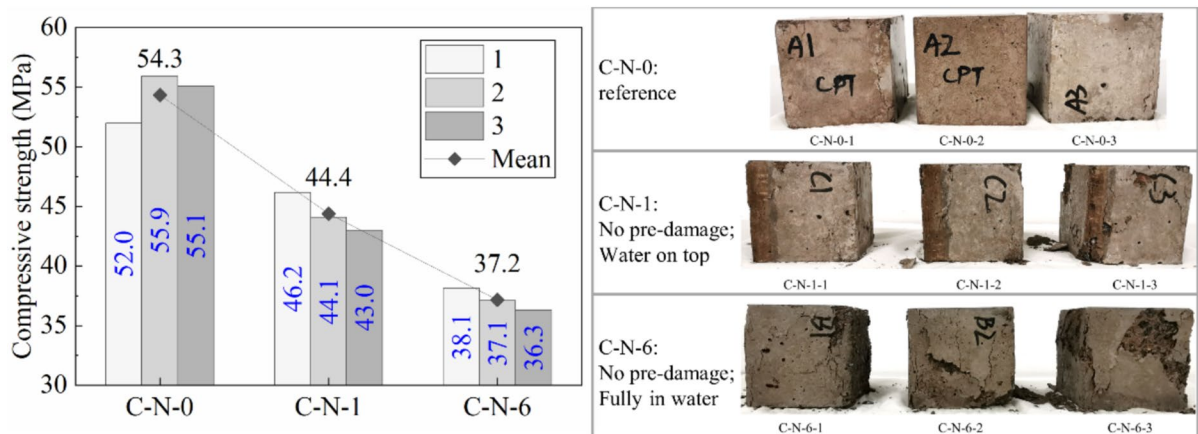
Fig. 10 Compressive strength and failure pattern of specimens subjected to freeze-thaw-cycles

and fully submerged during FTCs (C-N-6) exhibited intermediate and severe surface spalling, respectively. These observations underscore the correlation between water boundary conditions and internal frost damage, indicating that increased exposure of concrete surfaces to surrounding water leads to more severe internal frost damage and a significant reduction in the compressive strength of concrete. When exposed to the same freeze–thaw cycles, increased water exposure reduced compressive strength more significantly than tensile splitting strength.

3.4 Meso-scale: internal crack development

This section presents the meso-scale internal cracking of specimens detected through X-ray CT scanning. In Tables 4 and 5 each row depicts three representative cross-sections positioned at intervals of 25 mm, 50 mm, and 75 mm from the front surface of the scanned core extracted from a specimen (see Fig. 6a). The first and last cross-sections were closer to the external environment compared to the second (mid) cross-section. Each sub-figure presents a combination of original scanning images post unsharp masking (top-left and bottom-right quarters) and processed images with threshold adjustment (top-right and bottom-left quarters). The former displays the distribution of cement and aggregates, while the latter highlights the presence of internal cracks.

Table 4 illustrates internal cracking within specimens following wedge-splitting tests. The reference specimen, W-N-0-4, exhibited no observable cracks, indicating the absence of internal damage. This suggests an effective selection of drilling positions, as wedge-splitting tests did not impede the observation of internal cracks induced by frost damage. In contrast, in specimen W-N-6-1, fully submerged during FTCs, clear cracks were predominantly observed along aggregate-cement paste interfaces, which is a crucial sign of internal frost damage. Compared to W-N-6-1, pre-cracked specimen W-P-6-1 displayed not only cracks along aggregate-cement paste interfaces but also within the cement paste, suggesting a notable interaction between pre-cracking and FTCs in concrete. This phenomenon can also be observed by comparing the crack patterns of W-N-1-1 and W-P-1-1. These observations align with previous findings attributing pre-cracking to increased exposure
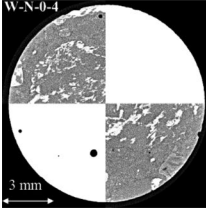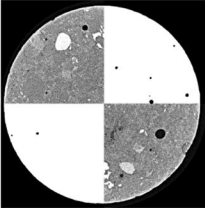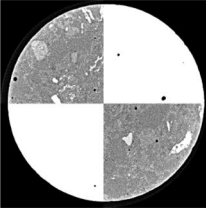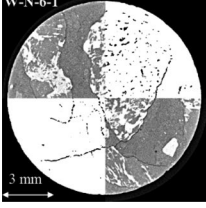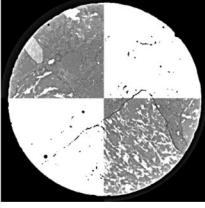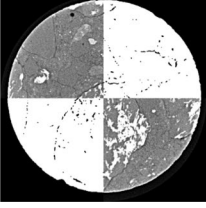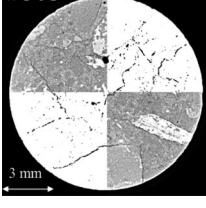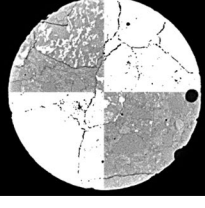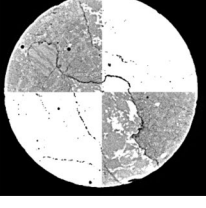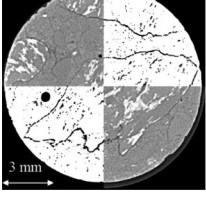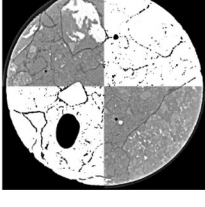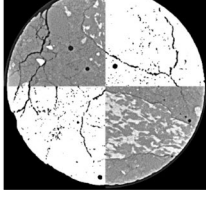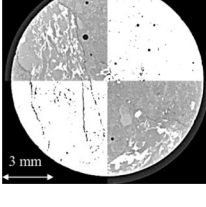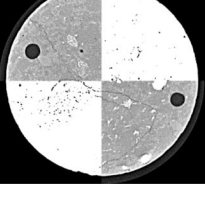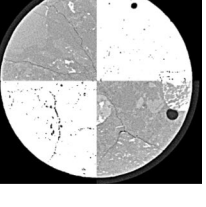
of concrete to the external environment, accelerating saturation and subsequent internal damage.

In specimen W-C-6-2, subjected to pre-compressive damage, severe crack development occurred in both the cement paste and aggregate-cement paste interfaces. This result agrees with the comparison of tensile strength shown in Fig. 9c, indicating that pre-compressive damage interacts with FTCs, leading to more severe internal damage in concrete compared to the scenario when there is no pre-damage (W-N-6-4). This observation verifies the previously stated indication that pre-compressive damage induces internal cracks in concrete, thereby accommodating more water. During FTCs, the extra water freezes and expands, in turn causing more internal cracks. The above-mentioned phenomena underscore the role of pre-damage in inducing internal cracks that amplify water ingress during FTCs, leading to exacerbated damage.
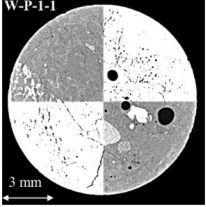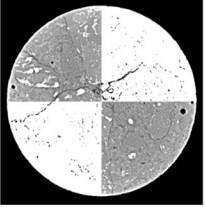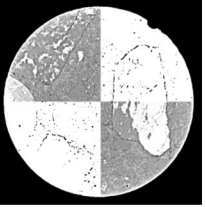
The influence of water boundary conditions on internal frost damage was further studied by comparisons of specimens W-N-6-1 and W-N-1-1 (both without pre-damage, fully submerged /with water maintained on top), as well as W-P-6-1 and W-P-1-1 (both pre-cracked, fully submerged / with water maintained on top). In specimens with water maintained on top (W-N-1-1 and W-P-1-1), crack propagation predominantly occurred along the aggregate-cement paste interfaces. However, these cracks exhibited slightly lower visibility and density compared to specimens fully submerged in water (W-N-6-1 and W-P-6-1), indicating that more surrounding water results in more internal frost damage.

The interaction between water boundary conditions and FTCs was elaborated through a comparison of cubic specimens (C-N-0-4, C-N-6-4, and C-N-1-4), as depicted in Table 5. Notably, unlike their counterparts in the same groups, these specimens were exclusively employed for X-ray CT scanning and were not subjected to compression tests. In the case of specimen C-N-6-4, fully submerged in water, cracks were observed across the cross-sections, predominantly along the aggregate-cement paste interfaces. Conversely, in specimen C-N-1-4, with water maintained on top, cracks were less pronounced, albeit still observable along these interfaces. These findings emphasise that more surrounding water content allows for more water to be absorbed into concrete pore systems, exacerbating internal frost damage
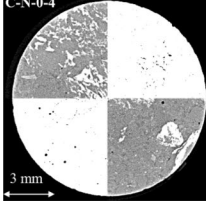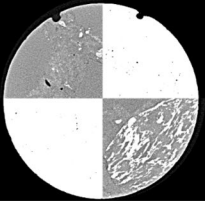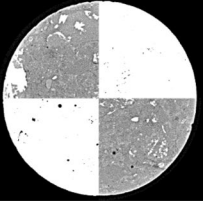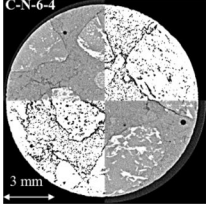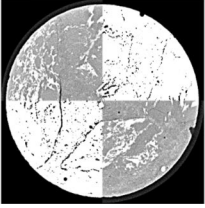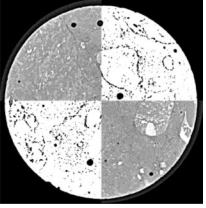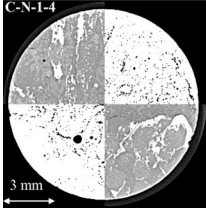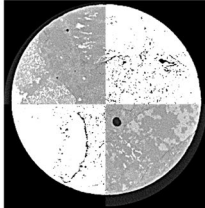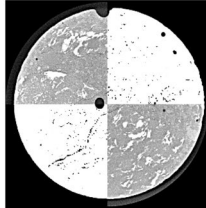
Table 4 Internal cracking within drilled cores of specimens after wedge-splitting tests

Specimens	Position of the sections at the drilled cores (from the front surface, mm)		
	25	50	75
W-N-0-4 (reference)			
W-N-6-1 (no pre-damage, fully submerged)			
W-P-6-1 (pre-cracked, fully submerged)			
W-C-6-2 (pre-compressed, fully submerged)			
W-N-1-1 (no pre-damage, water on top)			

Table 4 (continued)

Specimens	Position of the sections at the drilled cores (from the front surface, mm)		
	25	50	75
W-P-1-1 (pre-cracked, water on top)			

Table 5 Internal cracking within drilled cores of cubic specimens

Specimens	Position of the sections at the drilled cores (from the front surface, mm)		
	25	50	75
C-N-0-4 (reference)			
C-N-6-4 (no pre-damage, fully submerged in water)			
C-N-1-4 (no pre-damage, water on top)			

and leading to a subsequent decrease in compressive strength, as presented in Fig. 10.

The results of this study have significant implications for structural and construction engineering, particularly in cold regions where FTCs pose a severe threat to structural durability. The findings highlight the critical role of pre-damage and water boundary conditions in accelerating concrete deterioration, providing a foundation for predictive models that assess concrete performance under

combined environmental effects and mechanical stresses. Additionally, the dual-scale approach can be used by practitioners to identify critical damage thresholds and optimise maintenance schedules, ensuring the durability of existing concrete structures. The integration of DIC and portable X-ray CT imaging also demonstrates a practical diagnostic toolset for evaluating both surface-level and internal damage in concrete components, which can potentially be adapted for on-site applications.

4 Conclusions

This study investigates internal frost damage in concrete structures under realistic conditions, employing a dual-scale experimental approach to examine the interaction between pre-damage, water boundary conditions, and frost damage. Concrete specimens were pre-damaged and subjected to various well-defined water boundary conditions during Freeze-Thaw Cycles (FTCs), followed by macro-scale tests including wedge-splitting and compression tests to assess the interactive effects on the mechanical properties of concrete. Additionally, meso-scale X-ray CT scanning monitored internal crack development, while embedded temperature probes tracked internal temperature changes. The main findings of this study are summarised below.

At the macro-scale:

- The combined effects of pre-cracking and internal frost damage led to a greater reduction in the splitting tensile strength of concrete compared to the impact of internal frost damage alone.
- Similarly, the interactive effects of pre-compressive damage and internal frost damage resulted in a further reduction in the splitting tensile strength of concrete compared to internal frost damage alone.
- Increased water exposure during FTCs reduced both the splitting tensile strength and compressive strength of concrete, with a less significant impact on splitting tensile strength. Additionally, the increased water exposure resulted in a more diffused crack pattern and a slight increase in tensile ductility.

At the meso-scale:

- Specimens subject to the interactive effects of pre-damage (pre-cracking or pre-compressive damage) and FTCs showed internal cracks both along aggregate-cement paste interfaces and within cement paste.
- Specimens without pre-damage but subjected to FTCs showed internal cracks propagating mostly along aggregate-cement interfaces.
- Reference specimens without pre-damage or FTCs showed no internal cracks.
- Specimens fully submerged in water during FTCs showed more internal cracks than those with water on top.

Temperature change:

Temperature changes within concrete during freeze and thaw cycles exhibited distinct patterns depending on the water boundary conditions.

As a concluding remark, the results highlight the critical interaction between pre-damage, water boundary conditions, and internal frost damage on the durability performance of concrete. These findings provide valuable insights for improving the durability and design of concrete structures in frost-prone environments. Moreover, the well-defined water boundary conditions used during FTCs, together with the dual-scale settings in this experiment are ideal for calibrating numerical models of heat transfer and mechanical degradation in concrete subjected to internal frost damage. These findings can contribute to the development of more durable concrete mixes, the refinement of construction practices, and the optimisation of maintenance strategies, ultimately strengthening the resilience of concrete structures in cold regions.

Further research is needed to enhance the understanding of the phenomena involved. Valuable experimental studies could include extensions of this work at the micro-scale or investigations into the combined effects of other deteriorating factors, such as steel corrosion. Numerical studies could focus on multi-scale simulations of the crack propagation caused by the interplay between pre-damage and frost damage.

Data availability All data generated or used during the study appear in the submitted article.

Declarations

Conflict of interest The authors declare that they have no conflict of interest.

References

1. Pakkala TA et al (2016) Climate change effect on deterioration of concrete structures in Finland. Life-cycle of engineering systems. CRC Press, Cambridge, pp 1353–1359
2. Nasr A et al (2019) Bridges in a changing climate: a study of the potential impacts of climate change on bridges and their possible adaptations. Struct Infrastruct Eng 16(4):738–749
3. Fagerlund G (2004) A service life model for internal frost damage in concrete, in Report TVBM. 2004: Division of building materials, LTH, Lund University
4. Hanjari KZ, Utgenannt P, Lundgren K (2011) Experimental study of the material and bond properties of frost-damaged concrete. Cem Concr Res 41(3):244–254
5. Hanjari KZ, Kettil P, Lundgren K (2013) Modelling the structural behaviour of frost-damaged reinforced concrete structures. Struct Infrastruct Eng 9(5):416–431
6. Basheer L, Kropp J, Cleland DJ (2001) Assessment of the durability of concrete from its permeation properties: a review. Constr Build Mater 15(2–3):93–103
7. Wang X et al (2010) Analysis of climate change impacts on the deterioration of concrete infrastructure – Part 1: mechanisms, practices, modelling and simulations. CSIRO Climate adaptation flagship
8. Shi X et al (2012) Durability of steel reinforced concrete in chloride environments: an overview. Constr Build Mater 30:125–138
9. Zheng X et al (2022) Research progress of the thermo-physical and mechanical properties of concrete subjected to freeze-thaw cycles. Constr Build Mater. https://doi.org/10.1016/j.conbuildmat.2022.127254
10. Lu J et al (2017) Dynamic compressive strength of concrete damaged by fatigue loading and freeze-thaw cycling. Constr Build Mater 152:847–855
11. Kosior-Kazberuk M (2013) Variations in fracture energy of concrete subjected to cyclic freezing and thawing. Arch Civil Mech Eng 13(2):254–259
12. Ma Z, Zhao T, Yang J (2017) Fracture behavior of concrete exposed to the freeze-thaw environment. J Mater Civil Eng. https://doi.org/10.1061/(ASCE)MT.1943-5533.0001901
13. Jin M et al (2017) Characterization of internal damage of concrete subjected to freeze-thaw cycles by electrochemical impedance spectroscopy. Constr Build Mater 152:702–707
14. Rosenqvist M, Fridh K, Hassanzadeh M (2016) Macroscopic ice lens growth in hardened concrete. Cem Concr Res 88:114–125
15. Sun W et al (1999) Damage and damage resistance of high strength concrete under the action of load and freeze-thaw cycles. Cem Concr Res 29(9):1519–1523
16. Sun W et al (1999) Damage and its restraint of concrete with different strength grades under double damage factors. Cement Concr Compos 21(5–6):439–442
17. Bao J et al (2020) Coupled effects of sustained compressive loading and freeze-thaw cycles on water penetration into concrete. Struct Concr. https://doi.org/10.1002/suco.201900200
18. Fagerlund G (1977) The critical degree of saturation method of assessing the freeze/thaw resistance of concrete. Matériaux et Construction 10:217–229
19. Hassanzadeh M, Fagerlund G (2006) Residual strength of the frost-damaged reinforced concrete beams. In: III European conference on computational mechanics. Springer, Dordrecht, Netherlands
20. Rong X-L et al (2022) Seismic performance of reinforced concrete beams under freeze-thaw cycles. J Build Eng 60:103979
21. Shang HS, Song YP (2006) Experimental study of strength and deformation of plain concrete under biaxial compression after freezing and thawing cycles. Cem Concr Res 36(10):1857–1864
22. Wang Z et al (2014) Relative humidity and deterioration of concrete under freeze–thaw load. Constr Build Mater 62:18–27
23. Jiang L et al (2015) Durability of concrete under sulfate attack exposed to freeze–thaw cycles. Cold Reg Sci Technol 112:112–117

24. Zhu X et al (2022) Evaluation of fracture behavior of high-strength hydraulic concrete damaged by freeze-thaw cycle test. Constr Build Mater 321:126346

25. Wang Z et al (2021) Multiscale modeling and simulation of ice-strengthening effects in mesocracks of saturated frost-damaged concrete under freezing temperature. J Mater Civil Eng. https://doi.org/10.1061/(ASCE)MT.1943-5533.00034503

26. Hanjari KZ (2008) Material and bond properties of frost-damaged concrete, Report 2008:10. 2008: Chalmers University of Technology

27. Cui F-K et al (2017) Mechanical and failure criteria of air-entrained concrete under triaxial compression load after rapid freeze-thaw cycles. Adv Mater Sci Eng 2017:1–8

28. Wang B, Wang F, Wang Q (2018) Damage constitutive models of concrete under the coupling action of freeze-thaw cycles and load based on Lemaitre assumption. Constr Build Mater 173:332–341

29. Han N, Tian W (2018) Experimental study on the dynamic mechanical properties of concrete under freeze–thaw cycles. Struct Concr 19(5):1353–1362

30. Cao D et al (2021) Experimental study on the effect of freeze-thaw cycles on axial tension and compression performance of concrete after complete carbonation. Adv Civil Eng 2021:1–16

31. Zhu X, Chen X, Ning Y (2023) Experimental and numerical research on cyclic tensile performance of high-strength hydraulic concrete subjected to freeze–thaw damage. Int J Fatigue. https://doi.org/10.1016/j.ijfatigue.2023.107703

32. Robuschi S et al (2021) A closer look at corrosion of steel reinforcement bars in concrete using 3D neutron and X-ray computed tomography. Cement Concr Res. https://doi.org/10.1016/j.cemconres.2021.106439

33. Alhede A et al (2023) A two-stage study of steel corrosion and internal cracking revealed by multimodal tomography. Constr Build Mater. https://doi.org/10.1016/j.conbuildmat.2023.132187

34. Tian W, Han N (2018) Pore characteristics (>0.1 mm) of non-air entrained concrete destroyed by freeze-thaw cycles based on CT scanning and 3D printing. Cold Regions Sci Technol 151:314–322

35. Zhou Z et al (2019) On the modeling of tensile behavior of ultra-high performance fiber-reinforced concrete with freezing-thawing actions. Composit Part B: Eng 174:106983

36. Krstic M et al (2020) Freeze-thaw resistance and air-void analysis of concrete with recycled glass-pozzolan using x-ray micro-tomography. Materials (Basel) 14(1):154

37. Tian Z et al (2022) Microstructure and damage evolution of hydraulic concrete exposed to freeze–thaw cycles. Constr Build Mater 346:128466

38. Maus S et al (2023) X-ray micro-tomographic imaging and modelling of saline ice properties in concrete frost salt scaling experiments. Cold Regions Sci Technol 208:103780

39. Brühwiler E, Wittmann FH (1990) The wedge splitting test, a new method of performing stable fracture mechanics tests. Eng Fract Mech 35(1):117–125

40. Neuner M, Smaniotto S, Hofstetter G (2022) A modified wedge splitting test for susceptible quasi-brittle materials. Constr Build Mater 326:126733

41. CEN, Eurocode 2: design of concrete structures-part 1–1: general rules and rules for buildings. 2005: Brussels

42. Tang L, Petersson PE (2004) Slab test: freeze/thaw resistance of concrete—Internal deterioration. Mater Struct 37(10):754–759

43. CEN, EN 12390-3 Testing hardened concrete - Part 3: Compressive strength of test specimens. 2019

44. Schindelin J et al (2012) Fiji: an open-source platform for biological-image analysis. Nat Methods 9(7):676–682

45. Ridler T, Calvard S (1978) Picture thresholding using an iterative selection method. IEEE Trans Syst Man Cybern 8(8):630–632

46. Pålbrink L, Rydman O (2013) Frysning av betong under inverkan av tvång: en experimentell studie av frostens inverkan på betongkonstruktionerna i slutförvaret för kortlivat radioaktivt avfall efter en permafrost. Rapport TVBM (5000-serie)